

Effect of aging and alkali activator on the porous structure of a geopolymer

Prune Steins,^{a,b} Arnaud Poulesquen,^{a*} Fabien Frizon,^a Olivier Diat,^c Jacques Jestin,^d Jérémy Causse,^c David Lambertin^a and Sylvie Rossignol^b

^aCEA, DEN, DTCD/SPDE/LP2C, 30207, Bagnols sur Cèze, France, ^bGEMH, Ecole Nationale Supérieure de Céramique Industrielle–Limoges, Limoges, France, ^cICSM, Institut de Chimie Séparative de Marcoule UMR 5257 (CEA/CNRS/UM2/ENSCM), 30207, Bagnols sur Cèze, France, and ^dLaboratoire Léon Brillouin CEA/CNRS, CEA Saclay, 91191 Gif sur Yvette, France.
Correspondence e-mail: arnaud.poulesquen@cea.fr

Nitrogen sorption and small- and wide-angle X-ray and neutron scattering techniques were used to study the porous structure of geopolymers, inorganic polymers synthesized by reaction of a strongly alkaline solution and an aluminosilicate source (metakaolin). The effects of aging and the use of alkali activators (Na^+ , K^+) of different sizes were investigated at room temperature. The influence of aging time on the microstructure of both geopolymer matrixes was verified in terms of pore volume and specific surface area. The results suggested a refinement of the porosity and therefore a reduction in the pore volume over time. Regardless of the age considered, some characteristics of the porous network such as pore size, shape and distribution depend on the alkali activator used. Whatever the technique considered, the potassium geopolymer has a greater specific surface area than the sodium geopolymer. According to the scattering results, the refinement of the porosity can be associated with, first, a densification of the solid network and, secondly, a partial closure of the porosity at the nanometre scale. The kinetics are much slower for the sodium geopolymer than for the potassium geopolymer in the six months of observation.

© 2014 International Union of Crystallography

1. Introduction

The term ‘geopolymer’ denotes a class of amorphous three-dimensional aluminosilicate binder materials, formed at low temperature (Davidovits, 1991). These inorganic polymers are synthesized by the reaction of a strongly alkaline solution with an aluminosilicate source such as metakaolin (Duxson *et al.*, 2007). The formation of the geopolymer proceeds according to a mechanism of dissolution/restructuring/polymerization, which leads to a consolidated material (Prud’homme *et al.*, 2011; Phair & van Deventer, 2001). Geopolymers consist of a polymeric Si–O–Al framework. The chemical composition of geopolymers is similar to that of zeolite structures, but the final solid is typically X-ray amorphous or semi-crystalline (Fernandez-Jimenez *et al.*, 2005; Provis *et al.*, 2005).

A potential field of application of geopolymer materials is in immobilization of heavy metals and low-level nuclear waste (Palomo & Palacios, 2003; Fernandez Jimenez *et al.*, 2004; Desbats-Le Chequer & Frizon, 2011; Xu *et al.*, 2006). Indeed, geopolymers are considered as potential matrices to immobilize reactive metallic waste from UNGG (Natural Uranium Graphite Gas) reactors (Rooses *et al.*, 2013). Currently, the alkali silicate solutions of choice both in research and in industry are KOH or NaOH solutions owing to their performance, cost and availability. The influence of the nature and

the concentration of these alkali ions on physical and chemical properties has been investigated in recent work (Lee & van Deventer, 2002; Poulesquen *et al.*, 2011; Steins *et al.*, 2012; Kriven *et al.*, 2008; van Jaarsveld & van Deventer, 1999; Duxson *et al.*, 2006a).

According to the literature, geopolymers include a large volume of micro- and mesopores (Duxson *et al.*, 2005; Kriven *et al.*, 2007; Maitland *et al.*, 2011). The pore size distribution is wide and non-uniform (Maitland *et al.*, 2011). Several authors relate a total porosity of about 40%, with an average pore radius below 10 nm (Duxson *et al.*, 2005; Bell & Kriven, 2004; Kriven *et al.*, 2008).

However, this pore size distribution is highly dependent on the composition of the aluminosilicate source and of the alkali silicate solution. First, Duxson and co-authors showed that an increase in the size of the alkali activator yields a decrease in the pore size and an increase in the number of pores. Therefore, the microstructure of geopolymers is highly porous for Si/Al ratios ≤ 1.40 but largely homogeneous with small pores for Si/Al ≥ 1.65 (Duxson *et al.*, 2005, 2006b).

Temperature has an effect on the pore size distribution: with increasing temperature, the proportion of fine porosity decreases (Vance *et al.*, 2008), the collapse of pores is promoted and therefore the BET (Brunauer–Emmet–Teller) surface area is reduced (Ismail *et al.*, 2013). Finally, an excess

Table 1

Chemical composition of metakaolin.

Oxides	SiO ₂	Al ₂ O ₃	CaO	Fe ₂ O ₃	TiO ₂	K ₂ O	Na ₂ O	MgO
% weight	54.40	38.40	0.10	1.27	1.60	0.62	<0.20	<0.20

of water tends to create a matrix with larger pores (Steinerova *et al.*, 2010).

The aim of this work is to investigate the impact of aging and the nature of the alkali ion on the mesoscopic structure of the resulting geopolymer. For this purpose, several complementary techniques were used to characterize the porous structure of the geopolymer. Nitrogen sorption was used to measure the specific surface area and the pore size distribution as a function of time and of the nature of the alkali. This method requires a preliminary step of drying under vacuum to extract all the adsorbed molecules so that all of the porosity is accessible. Unlike nitrogen sorption, small- and wide-angle X-ray scattering (SWAXS), ultra-small-angle X-ray scattering (USAXS) and small-angle neutron scattering (SANS) have the advantage of being neither invasive nor destructive (Ramsay, 1993). Interfacial properties such as surface area (open and closed porosity), size and roughness (*i.e.* the fractal dimension) of pores constituting the geopolymer can be precisely determined using X-ray scattering techniques. In addition, the SANS technique with contrast variation is used to determine precisely the proportion of open and/or closed porosity and the change in the real specific surface area over time.

2. Materials and methods

2.1. Geopolymer synthesis

The metakaolin used was a Premix from Grace Construction Products. The chemical composition determined by X-ray fluorescence (XRF) is given in Table 1. Two different alkali hydroxide activating solutions were prepared by dissolving NaOH or KOH pellets (purity >99% from Merck) and amorphous silica (Tixosil 331, Rhodia) in Milli-Q water. Thus, two series of mixtures were prepared in the same molar ratios: 1:1.8:1:12 Al/Si/M/H₂O ($M = \text{Na or K}$). The mixing was performed in two steps. First, alkali silicate solutions were prepared by dissolving amorphous silica in alkali solution under magnetic stirring for 24 h. Geopolymer matrices were prepared by mechanically mixing the metakaolin with the alkali silicate solution for 20 min (Steins *et al.*, 2012). Then the geopolymer blocks were sliced with appropriate optimal thicknesses depending on the characterization used.

2.2. Nitrogen sorption

Samples of the geopolymer were stored in airtight containers before each measurement of nitrogen adsorption. Nitrogen adsorption measurements were performed using a Micromeritics ASAP 2020 instrument. The geopolymers were freeze-dried with liquid nitrogen before being introduced into the device. This technique is considered to minimize altera-

tions to the pore structure (Gallé, 2001). After the freeze-drying step, samples were degassed under vacuum with a temperature rise up to 623 K at 10 K min⁻¹ to desorb all traces of impurities on the material surface. The specific surface area was calculated using the BET method (Barrett *et al.*, 1951). Pore size distributions were obtained by the Barrett–Joyner–Halenda (BJH) method using the desorption branch.¹ The gas adsorption measurements were conducted on sodium and potassium geopolymers at different aging times (three, seven and 14 days and six months after synthesis).

2.3. SWAXS–USAXS experiments

X-ray scattering experiments were performed to determine the effect on the specific surface, at the nanometre scale, of the porosity created during the geopolymerization. One series of SWAXS measurements was carried out using Mo radiation ($\lambda = 0.071$ nm) on a bench built by Xenocs. Collimation was applied using a 12:∞ multilayer mirror coupled to two sets of scatterless slits (Forvis) and providing a 0.8 × 0.8 mm X-ray beam at the sample position. Scattering intensities were recorded on a large-area imaging-plate system (Mar345) and azimuthally averaged to obtain $I(q)$, the scattering being isotropic. The scattering vector modulus is defined as $q = (4\pi/\lambda)\sin\theta$, where 2θ is the scattering angle and λ is the wavelength of the incident radiation. A wide range of q (2×10^{-1} – 25 nm⁻¹) was covered as a result of the short sample-to-detector distance (735 mm) and off-centred detection. The X-ray flux and the efficiency of the detector were determined using a calibrated piece of high-density polyethylene. The absolute intensity was then obtained by taking into account the transmission (measured before each acquisition), the acquisition time (300 s for each measurement), the sample thickness, and the subtraction of the empty cell contribution and detector background.

Complementary X-ray measurements were carried out at the laboratory LIONS (Interdisciplinary Laboratory on Nanoscale and Supramolecular Organization) using a USAXS instrument for extending the detection to lower q values. The X-ray emitting source is a rotating copper anode ($\lambda = 0.154$ nm) and the covered q range is between 4×10^{-3} and 0.4 nm⁻¹ for this setup. The smearing effect due to slit collimation in the vertical direction was corrected using a homemade program (Lambard *et al.*, 1992). The raw intensities were corrected with the same treatments described previously for SAXS.

SAXS and USAXS were performed on thin plates of geopolymer (sodium and potassium) of about 500 μm thickness, at room temperature, one and six months after synthesis.

2.4. SANS experiments

The SANS technique was used for determining the real scattering length density of the geopolymers and to measure the fraction of closed and opened porosity by varying the contrast of the confined water within the geopolymer.

¹ Supporting information for this article is available from the IUCr electronic archives (Reference: RG5050).

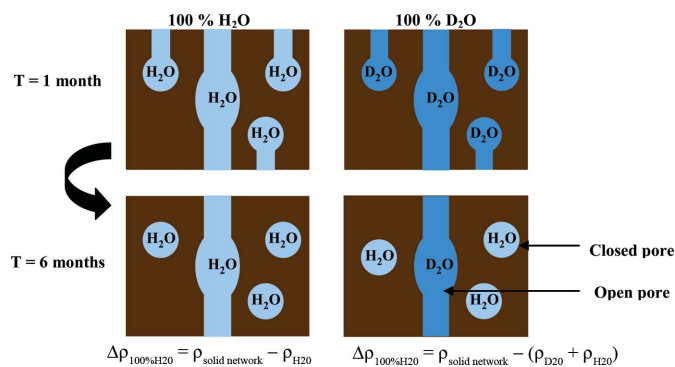


Figure 1
Diagram illustrating the closed porosity detection by the contrast variation experiment.

SANS experiments were performed on the PACE spectrometer at the Laboratoire Léon Brillouin (Orphée Nuclear Reactor, Saclay, France). PACE is a spectrometer for studying isotropic scattering. Experiments were performed for a single configuration ($\lambda = 5 \text{ \AA}$, sample–detector distance = 1.4 m) with a range of scattering vector modulus q from 3×10^{-1} to 3 nm^{-1} . The samples were sandwiched between 1–2 mm-thick quartz windows and maintained at 298 K. The treatment was carried out using the software *Pasinet* (Brület *et al.*, 2007). The absolute intensity was obtained by taking into account the transmission, the sample thickness and the contribution of the empty cell. The coherent background was estimated considering the amount of protonated water within and around the sample as well as those coming from the solid structure. Owing to the Porod law observed using the SAXS technique, a final correction was applied to get a q^{-4} decay for the wide-angle part of the SANS spectra. Then, the intensity was normalized by water scattering in order to correct for the inhomogeneities of the detector response.

To determine the surface areas and the open and closed porosity (principle detailed in Fig. 1), thin plates of sodium and potassium geopolymers with different aging times were immersed two times for 4 and 10 h in various H_2O – D_2O mixtures. The exchange time required to empty and refill the

pores with the new solvent H_2O – D_2O was checked by ICP dosage, taking care that no more solute was present in the pore solution. A few drops of solvent were added before introducing the sample of geopolymer between the quartz windows. This technique takes advantage of the different scattering length densities, ρ , for light water (H_2O) and heavy water (D_2O). These are $-0.558 \times 10^{10} \text{ cm}^{-2}$ for H_2O and $6.341 \times 10^{10} \text{ cm}^{-2}$ for D_2O at room temperature (Sears, 1992).

3. Results

3.1. Nitrogen adsorption (surface area, pore volume and size distribution)

Adsorption and desorption isotherms obtained at different times (three, seven and 14 days and six months) for the sodium- and potassium-based geopolymers are shown in Fig. 2.

All samples exhibit a distinct large hysteresis loop from 0.5 to 1.0 of relative partial pressure (P/P_0). The closeness of the hysteresis loop at $P/P_0 > 0.40$ indicates the absence of micropores and the formation of a well defined mesoporous texture (Radlinski *et al.*, 2004; Sharma *et al.*, 2002). According to IUPAC classification, the nitrogen adsorption–desorption isotherms show a typical type IV sorption behaviour with mixed type hysteresis loops (H1 + H2) (Rouquerol *et al.*, 2003; Kuznetsova *et al.*, 2012). The features of a hysteresis loop of type 1 on a loop of type 2 are usually attributed to a difference in mechanism between the condensation and evaporation processes occurring in interconnected pores with narrow necks and wide voids, often called ‘ink-bottle pores’ (Brunauer *et al.*, 1938; Leofanti *et al.*, 1998; Mami *et al.*, 2008).

For both alkali ions, aging time has an impact on pore volume, specific surface area and hysteresis shape. Whatever the nature of the alkali cation used in the synthesis, between three days and six months, the pore volume decreases from 0.23 to 0.13 $\text{cm}^3 \text{ g}^{-1}$ for the sodium geopolymer and from 0.34 to 0.26 $\text{cm}^3 \text{ g}^{-1}$ for the potassium geopolymer (Table 2). The BET surface area follows the same trend for both geopolymers. Between three days and six months, it decreases from 62 to 36 $\text{m}^2 \text{ g}^{-1}$ for the sodium geopolymer and from 155 to 106 $\text{m}^2 \text{ g}^{-1}$ for the potassium geopolymer (see Table 2).

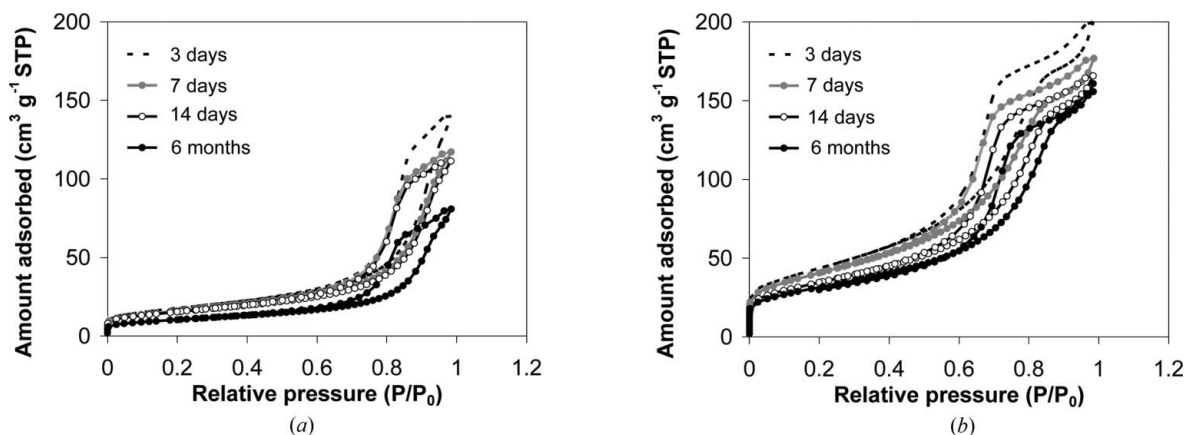


Figure 2
Nitrogen adsorption–desorption isotherms for the sodium geopolymer (a) and the potassium geopolymer (b) at different aging times: $t = 3, 7, 14 \text{ d}$ and 6 months (STP: standard temperature and pressure).

Table 2

Specific surface area, pore volume and pore diameter measured by nitrogen adsorption for sodium and potassium geopolymers at different aging times: $t = 3, 7, 14$ d and 6 months.

Time	Sodium geopolymer			Potassium geopolymer		
	S_{BET} ($\text{m}^2 \text{g}^{-1}$)	D_{pore} (\AA)	V_{pore} ($\text{cm}^3 \text{g}^{-1}$)	S_{BET} ($\text{m}^2 \text{g}^{-1}$)	D_{pore} (\AA)	V_{pore} ($\text{cm}^3 \text{g}^{-1}$)
3 d	62	112	0.23	155	62	0.34
7 d	58	102	0.19	145	60	0.30
14 d	54	102	0.18	123	65	0.28
6 months	36	107	0.13	106	73	0.26

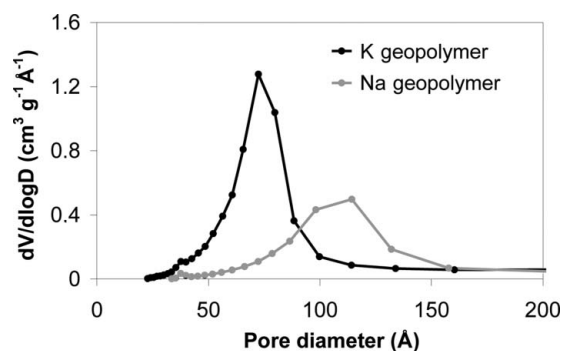
The hysteresis shape is much more affected by the alkali ion of the activating solution: the sorption branch is much more gradual and the inflection point on the adsorption branch ($P/P_0 = 0.85$) is more pronounced for the potassium geopolymer, whereas the hysteresis branches of the sodium geopolymer are quite parallel, with a less pronounced inflection point.

Between three days and six months, the hysteresis is closing for a relative pressure $P/P_0 > 0.85$. This effect is more pronounced for the potassium geopolymer than the sodium geopolymer (Fig. 2). Finally, the bend of the isotherm shifts towards higher pressures for the potassium geopolymer (from 0.46 to 0.61), whereas it remains substantially constant for sodium geopolymer (0.58 at three days and six months).

From these results, the potassium geopolymer adsorbs a larger volume of nitrogen than the sodium geopolymer: 1.25 versus $0.5 \text{ cm}^3 \text{g}^{-1} \text{\AA}^{-1}$, respectively, at six months (Fig. 3). In the same way, the BET surface area is much lower for the sodium geopolymer than for the potassium geopolymer whatever the level of aging (Table 2). Lastly, the pore size distribution is wider for the sodium than for the potassium geopolymer: at 6 months, the pore size distribution is between 50 and 200 \AA for the sodium and only between 25 and 85 \AA for the potassium geopolymer (Fig. 3).

3.2. SAXS–USAXS: geopolymer morphology

The use of SAXS and USAXS techniques provides additional information on the mesoscopic morphology of the geopolymers. Fig. 4 shows the combined SAXS and USAXS scattering data for both types of geopolymer and for meta-


Figure 3

BJH pore-size distribution for the sodium geopolymer and the potassium geopolymer at six months.

kaolin dispersed in water. The spectra of geopolymers can be divided into three regions for analysis (Cailleateau *et al.*, 2008):

(1) A first region at low q , where the three scattering curves overlap. In this region, the SAXS intensity $I(q)$ decreases as a function of q^{-D} , where the exponent D corresponds to the mass fractal dimension of the network structure (Tsao *et al.*, 2007). The slopes of the measured SAXS profiles reveal a mass fractal dimension of 2.8 for the network structure.

(2) A second region, for q between 0.3 and 1 nm^{-1} , characterized by a Porod law (Porod, 1952), differs from the dispersion of metakaolin because of the porous network with sharp interfaces created during the geopolymerization (Ledieu *et al.*, 2004). At large q , crystalline peak are observed whatever the system. These crystallized phases correspond to the unreacted metakaolin particles.

(3) An intermediate region around 10^{-1} nm^{-1} , corresponding to the transition between these regimes of interest.

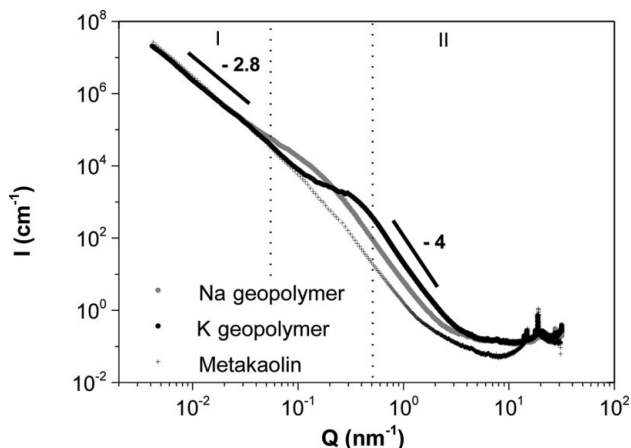
For $q < 0.03 \text{ nm}^{-1}$, the scattering intensity, which varies as $q^{-2.8}$, corresponds to the electronic density fluctuations of the amorphous part of the solid network. The exponent 2.8 can be associated with a mass fractal exponent characterizing a dense material. We have checked by scanning electron microscopy that particles of metakaolin are dispersed in the amorphous part of the geopolymer in the form of platelets of about few micrometres (Jämstorp *et al.*, 2010).

For q below 1 nm^{-1} , the intensity scattered by the geopolymer, which varies as q^{-4} , represents a well defined surface associated with the interface between voids filled with the solution and the solid network of the geopolymer (Steins *et al.*, 2012).

In Fig. 5, SAXS and USAXS data of sodium and potassium geopolymers aged by one and six months are plotted in the Porod representation [$I(q)q^4$ versus q].

A characteristic size of the porous network can be estimated by using in a crude approach a model of an assembly of polydisperse spheres with a lognormal distribution of radii.

$P(Q)$ is the form factor for a sphere of radius R :


Figure 4

Small-angle X-ray scattering. Scattered intensity versus scattering vector modulus for the sodium geopolymer, the potassium geopolymer and metakaolin at six months.

Table 3

Specific surface area measured by SAXS for sodium and potassium geopolymers at 1 and 6 months.

Time (month)	Electronic contrast	S_{SAXS} ($\text{m}^2 \text{g}^{-1}$) sodium geopolymer	S_{SAXS} ($\text{m}^2 \text{g}^{-1}$) potassium geopolymer
1	$\rho_{\text{solid network}} - \rho_{\text{water}}$	244 (10)	704 (20)
6		271 (4)	878 (20)
1	$\rho_{\text{solid network}} - \rho_{\text{air}}$	80 (10)	235 (20)
6		89 (4)	293 (20)

$$P(q) = \left\{ \frac{3[\sin(qR) - qR \cos(qR)]}{(qR)^3} \right\}^2 \quad (1)$$

The function $f(R, R_0, q)$ of a lognormal distribution for polydisperse spheres of radius R is given by

$$f(R, R_0, q) = \frac{1}{\text{Norm}} \exp \left\{ -\frac{1}{2\sigma^2} \left[\ln \left(\frac{R}{R_0} \right) \right]^2 \right\} \quad (2)$$

The distribution function $f(R, R_0, q)$ gives the proportion of pores with a radius R in a distribution of median radius R_0 with a standard deviation σ . Norm is a normalization factor.

Whatever the alkali used, aging of samples yields first a slight increase in the scattered intensity at low wavevector. Then, the pore size characterized by the radius of the sphere moves from $R = 2.7 \pm 1$ nm to $R = 3.4 \pm 1.3$ nm between one and six months for the potassium geopolymer, whereas a slight increase is observed for the sodium geopolymer: $R = 3.5 \pm 2$ nm at one month and $R = 3.9 \pm 2.4$ nm at six months. This change, observed for both geopolymers, would represent a slight increase in the size of the porous network. It is important to note that the polydispersity for the sodium geopolymer is very high (60%) as compared to that of the potassium geopolymer (38%).

Whatever the age, the scattered intensity is higher for the potassium geopolymer than for the sodium geopolymer and the levelling off at higher wavevectors is more pronounced for the potassium geopolymer.

The range of scattering vector where Iq^4 is constant (transition between the two regimes) depends on the cation used in

the synthesis of the geopolymer. For large scattering angles, the Porod regime is checked for both geopolymers and the area density of the pores, Σ_{pores} , may be estimated from the relation (Sears, 1992)

$$\Sigma_{\text{pores}} = \frac{S}{V} = \frac{\lim I(q)_{q \rightarrow \infty} q^4}{2\pi \Delta\rho^2}, \quad (3)$$

where S/V is the specific area per volume and $\Delta\rho^2$ is the electronic contrast between the scattering length density of the solid network of the geopolymer, $\rho_{\text{solid network}}$, and the scattering length density of the pore fluid, $\rho_{\text{pore fluid}}$.

In this system, the composition of the pore solution is unknown. Consequently, two electronic contrasts were considered. In both cases, $\rho_{\text{solid network}}$ was calculated by assuming that the solid network is a mix of metakaolin, silica from the activating solution and the alkali, which keeps the electric balance in the matrix neutral. In the first case, $\rho_{\text{pore fluid}}$ was calculated by assuming that the pore fluid is pure water, $\rho_{\text{pore water}}$. According to the literature, the pore solution still contains ions but in lower concentrations than in the initial activating solution (Lloyd *et al.*, 2010).

In the second case, $\rho_{\text{pore fluid}}$ was calculated by assuming that the pores are filled with air, $\rho_{\text{pore air}}$. This case was considered because the surface of the pellets appeared dehydrated.

The specific surface area ($\text{m}^2 \text{g}^{-1}$) is thus obtained by dividing the area density of the pores (m^{-1}) [equation (1)] by the density of geopolymer (2.43 g cm^{-3}). The specific surfaces obtained by SAXS for both geopolymers at different ages for different electronic contrasts are summarized in Table 3.

The specific surfaces obtained by considering that the pore fluid is water are much higher than those obtained by assuming that the pores are filled with air (271 *versus* 89 $\text{m}^2 \text{g}^{-1}$ for the sodium geopolymer and 878 *versus* 293 $\text{m}^2 \text{g}^{-1}$ for the potassium geopolymer at six months). Whatever the electronic contrast used, the specific surface is much higher for the potassium geopolymer than for the sodium geopolymer and slightly increases with time for both cations. It increases from 244 to 271 $\text{m}^2 \text{g}^{-1}$ for the sodium geopolymer and from 704 to 878 $\text{m}^2 \text{g}^{-1}$ for the potassium

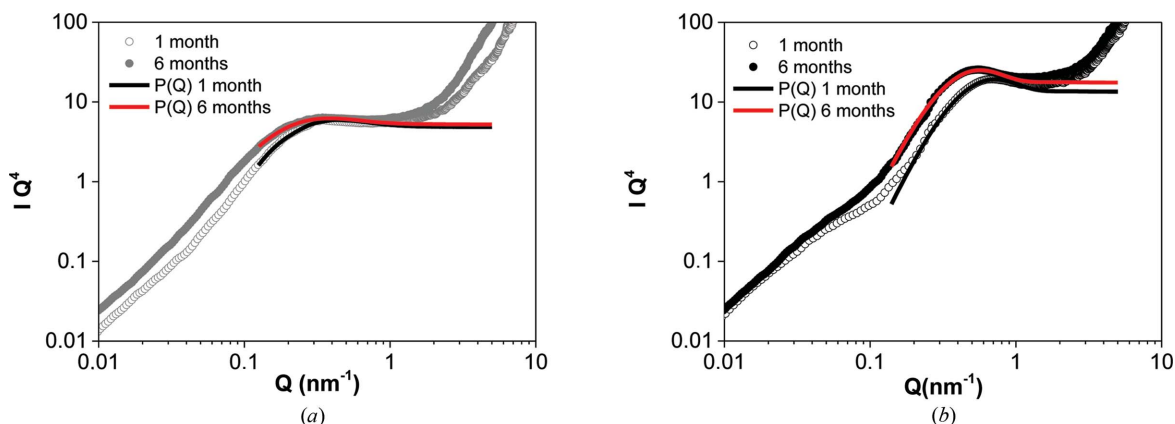


Figure 5

Small-angle X-ray scattering. Porod plots of the sodium geopolymer (a) and the potassium geopolymer (b) at one and six months. The experimental curves were modelled by *SasView* (<http://www.sasview.org/>).

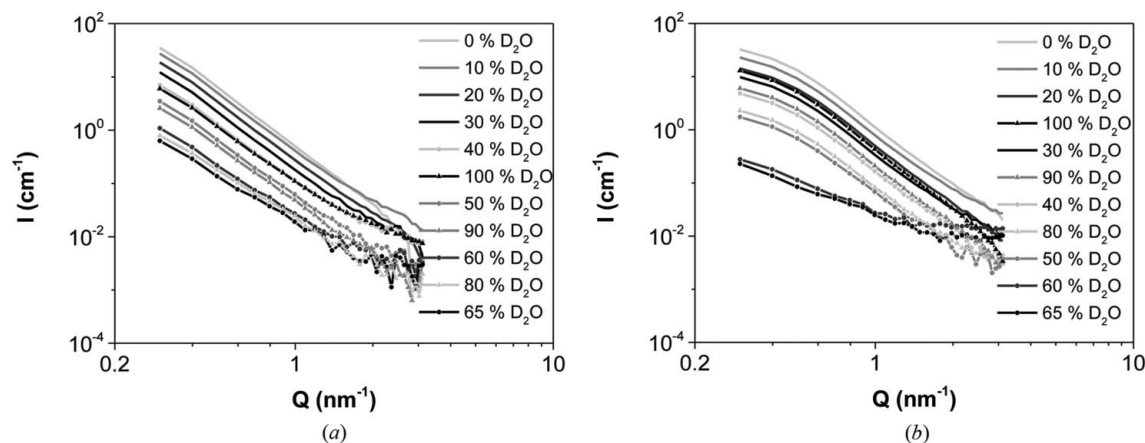


Figure 6 Small-angle neutron scattering. Scattered intensity *versus* scattering vector modulus with different solution isotopic compositions (H_2O – D_2O) for the sodium geopolymer (a) and for the potassium geopolymer (b).

geopolymer if the pore fluid is water and from 80 to 89 $\text{m}^2 \text{g}^{-1}$ for the sodium geopolymer and from 235 to 293 $\text{m}^2 \text{g}^{-1}$ for the potassium geopolymer if the pores are filled with air.

3.3. SANS results

Neutron scattering with contrast matching by isotopic exchange is a very powerful technique to get information about the properties of porous solids, namely to obtain the scattering length density of geopolymers and to measure the proportion of open and/or closed pores.

First, the pore solution of a one-month-aged geopolymer was replaced by different H_2O – D_2O mixtures in order to determine the isotopic composition corresponding to the scattering length density of the geopolymer. Fig. 6 shows geopolymer scattering curves for different H_2O – D_2O mixtures and for both alkalis. The scattering curve of the geopolymer was obtained by subtracting the contribution of the solvent. Analysis of the scattering curves was then performed in the same way as for X-ray scattering. The signals observed in Fig. 6 are the contribution of the solid network and of the solvent trapped in the geopolymer pores (Maitland *et al.*, 2011). The immersion of the geopolymer in various solvents yields a variation in the scattered intensity for two reasons: first the background attributed to incoherent scattering from varying amounts of hydrogen in the solvent, and secondly the scattering contrast between the pore solution and the solid network. The intensity, which varies as q^{-4} within the range $5 \times 10^{-1} < q < 1 \text{ nm}^{-1}$, indicates the presence of a Porod regime, which allows an assessment of the geopolymer specific surface area. The H_2O – D_2O mixture for which the broadcast signal disappears was determined by plotting the variation of the square root of the intensity scattered by the sample of geopolymer at $q = 5.97 \times 10^{-2} \text{ nm}^{-1}$ as a function of the D_2O volume fraction in the solution (Fig. 7). The isotopic mixtures corresponding to extinction in terms of the contrast of the geopolymer network are $\text{H}_2\text{O}/\text{D}_2\text{O}$: 29.3/70.7 (v/v) and $\text{H}_2\text{O}/\text{D}_2\text{O}$: 34.8/65.2 (v/v) for sodium and potassium, respectively. From these extinction mixtures, the geopolymer scattering

length densities were calculated and the neutron contrast between the geopolymer networks and the pore solutions were deduced for both systems (Table 4).

The intensities scattered by pellets from the same mix were compared at one and six months. One was immersed in 100% H_2O and the other in 100% D_2O . The curves were normalized by the neutron contrast between the solid network of the geopolymer and the pore solution composed of H_2O or D_2O (Fig. 8). The red curve represents the intensity scattered by the geopolymer pellet immersed in 100% H_2O and the black one the intensity scattered by the pellet immersed in 100% D_2O . According to Fig. 8, one month after the synthesis, the ‘ H_2O ’ and ‘ D_2O ’ curves overlap for the sodium geopolymer, while the intensity of the ‘ D_2O ’ curve is slightly higher for the potassium geopolymer. At six months, the ‘ H_2O ’ and the ‘ D_2O ’ scattering curves do not overlap anymore for either alkali activator. The intensity of the black curve is thus certainly the result of two contributions: the scattering contrast between the solid network and (i) the accessible and

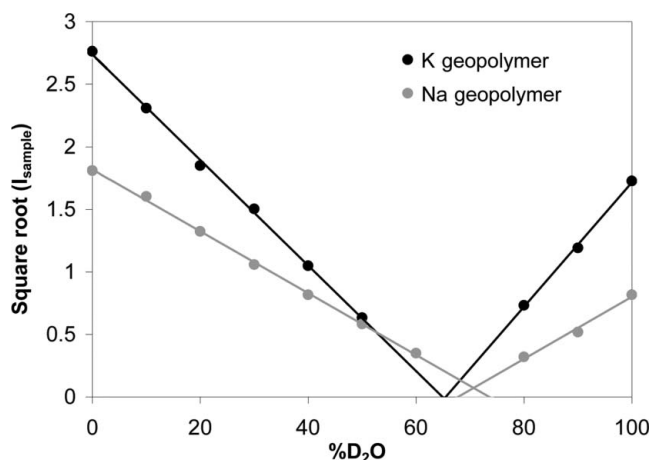


Figure 7 Small-angle neutron scattering. Variation of the square root of the intensity scattered by the sodium geopolymer and the potassium geopolymer as a function of the D_2O volume fraction.

Table 4

Extinction mixture associated with the neutron scattering length density and the specific surface area of sodium and potassium geopolymers at one and six months.

	Sodium geopolymer	Potassium geopolymer
Extinction mixture H ₂ O–D ₂ O	29.3–70.7	34.8–65.2
Scattering length density (cm ⁻²)	4.37 × 10 ¹⁰	3.98 × 10 ¹⁰
Specific surface area (m ² g ⁻¹)		
1 month	107 (5)	342 (3)
6 months	107 (5)	342 (3)

opened porosity and (ii) the closed porosity for which no solution exchange was possible (see Fig. 1).

Finally, using equation (1) and the intensity scattered by the pellets immersed in H₂O at one and six months, specific surfaces for both geopolymers were calculated (Table 4). At one month, the specific surfaces were found to be equal to 107 m² g⁻¹ for the sodium geopolymer versus 342 m² g⁻¹ for the potassium geopolymer. Between one and six months, the characteristic curves of samples immersed in H₂O have the same intensity for both geopolymers. This means that the specific surface areas of geopolymers determined from these curves do not change over time (Table 4).

4. Discussion

4.1. Structural evolution for both geopolymers over time

Several structural changes are observed for both geopolymers over time: a decrease in the pore volume and specific surface area when using nitrogen adsorption. SANS results confirmed the appearance of a closed porosity that is not accessible to the solvent. The accessibility to pores decreases and this is certainly due to the refinement of the porosity induced by hydrolysis and dissolution reactions that still go on.

The surface area determined by nitrogen adsorption is lower than that derived from SAXS and SANS data. This is because these two techniques (scattering techniques and the nitrogen adsorption method) do not detect the same specific surface, especially in the case where the solid is obtained through a three-dimensional polymerization, which can appear very rough. Moreover the accessibility of partially closed pores by solution or gas is different (Radlinski *et al.*, 2004).

Unlike the nitrogen adsorption results, the specific surface area obtained by SAXS, calculated from the intensity curves and the electronic contrast, increases over time. We can propose two hypotheses:

(1) either the specific surface area can increase over time owing to the closure of channels, creating new interfaces,

(2) or there is a new electronic contrast between the solution and the geopolymer network – this variation can result from a change in the pore solution, composition (Lloyd *et al.*, 2010) or evaporation.

However, we observed that the specific surface areas of geopolymers determined by SANS do not change over time (Table 4). The specific surface area determined by SANS is more accurate than that derived from SAXS because no hypothesis about the geopolymer composition was necessary. Thus, the second assumption is more credible, with a partial dehydration of the porous structure. The specific surface area calculated by SAXS by assuming that pores were filled with air is indeed closer to those obtained by SANS analysis.

4.2. Influence of the alkali activator

Regardless of the age considered, some characteristics of the porous network depend on the alkali activator used. From the hysteresis form and the BJH curves, the shape and size of

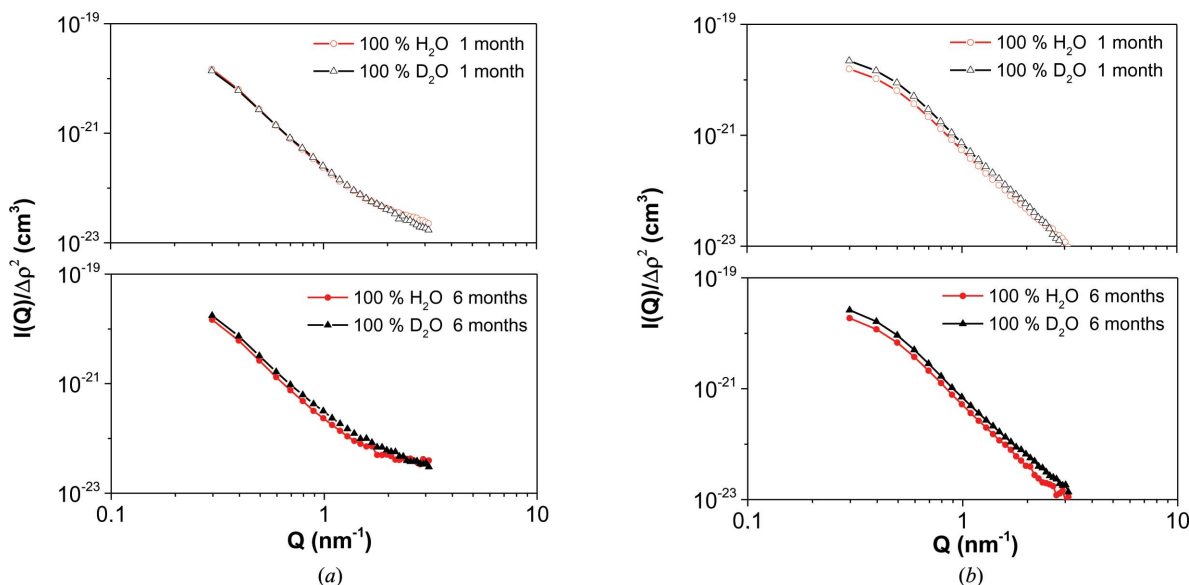


Figure 8

Small-angle neutron scattering. Scattered intensity versus scattering vector modulus with 100% H₂O and 100% D₂O for the sodium geopolymer (a) and for the potassium geopolymer (b) at one and six months.

pores are different. The sodium geopolymer has a single family of large and well defined pores (single hysteresis loop with parallel branches), while the potassium geopolymer has a family of small heterogeneous, highly connected pores (Figs. 2 and 3). This result is confirmed by SAXS (Fig. 5), where the pore size characterized by the radius of a polydisperse sphere is smaller for the potassium geopolymer than for the sodium geopolymer whatever the age considered. In addition, the intermediate region appears at a higher q value for potassium, suggesting that the characteristic pore size is smaller with a larger volume fraction according to the BET measurements. The pore size determined by SAXS measurement is in a very good agreement with the nitrogen adsorption experiments. The high polydispersity observed for sodium ($\sim 60\%$) confirms the BJH results, where the pore size distribution is wider for sodium than for potassium.

We also confirm that the mean pore size decreases whereas the total pore area increases with the potassium geopolymer in relation to the sodium geopolymer (Duxson *et al.*, 2005; Bell & Kriven, 2004). Consequently, whatever the technique considered, the potassium geopolymer has a greater specific surface area than the sodium geopolymer (Tables 2, 3 and 4) (van Jaarsveld & van Deventer, 1999). Finally, according to the SANS results, the potassium geopolymer already has a very small fraction of closed pores at one month, in contrast to the sodium geopolymer.

The alkali activator also affects the structural evolution of the geopolymer. Regarding the isotherms, the closure of the hysteresis at high pressures is more pronounced for the potassium geopolymer than for the sodium geopolymer. These results suggest that the porous structure becomes denser with a stronger effect for the potassium geopolymer. This densification could result from the dissolution and the recondensation of the geopolymer network (Tsao *et al.*, 2007; Cailleateau *et al.*, 2008; Girard *et al.*, 2008), which is certainly faster and favoured with the potassium geopolymer.

Concerning the pore size, the distribution is substantially invariant for sodium but seems to increase slightly for potassium between three days and six months (see Table 2). Moreover, the pore size characterized by the radius of the sphere (Fig. 5) increases more significantly for the potassium geopolymer than for the sodium geopolymer. This change between one and six months means that the characteristic sizes in the porous network are slightly larger for the potassium geopolymer and relatively invariant for the sodium geopolymer. This increase in the pore size for both geopolymers is related to a refinement of the porosity over time due to, for example, a constriction of some narrow channel.

5. Conclusion and outlook

Nitrogen sorption, SAXS and SANS were used to provide new information on the structural evolution of geopolymers. According to the results, the pores that are not accessible to these techniques represent a small part of the total porosity but tend to increase over time as a result of a refinement of the porosity. The refinement of the porosity can be associated

with, first, a densification of the solid network and, secondly, a partial closure of the porosity at the nanometre scale

The determination of the scattering length density of geopolymers by SANS allowed us to calculate precisely the specific surface areas. At one month, the specific surface areas determined by SAXS, by assuming that the pores were filled with air, and SANS are quite close. However, the increase in intensity of the SAXS curves suggests a partial dehydration of the porous structure over time.

Finally, the use of two alkali ions (Na^+ and K^+) differing by their size and by their kosmotropic or chaotropic properties allowed us to demonstrate that pore size, shape and distribution depend on the alkali activator. The potassium geopolymer has a greater specific surface area than the sodium geopolymer because the pores are smaller and more numerous. According to the scattering results, the kinetics are much slower for the sodium geopolymer than for the potassium geopolymer in the six months of observation.

To complement this study, extractions of pore solution would be necessary to obtain information about the composition over time. Furthermore, quasi-elastic scattering and NMR relaxometry techniques could be used to investigate confined water dynamics to provide more accurate information about the pore size, the closed/open porosity and the pore surface composition (Briman *et al.*, 2012).

The authors are grateful to Adrien Gerenton for BET measurements, and Olivier Spalla and Olivier Tache for USAXS measurements.

References

- Barrett, E. P., Joyner, L. G. & Halenda, P. P. (1951). *J. Am. Chem. Soc.* **73**, 373–380.
- Bell, J. L. & Kriven, W. M. (2004). *Microsc. Microanal.* **10**, 590–591.
- Briman, I. M., Rébiscoul, D., Diat, O., Zanotti, J.-M., Jollivet, P., Barboux, P. & Gin, S. (2012). *J. Phys. Chem. C*, **116**, 7021–7028.
- Brûlet, A., Lairez, D., Lapp, A. & Cotton, J.-P. (2007). *J. Appl. Cryst.* **40**, 165–177.
- Brunauer, S., Emmett, P. H. & Teller, E. (1938). *J. Am. Chem. Soc.* **60**, 309–319.
- Cailleateau, C., Angeli, F., Devreux, F., Gin, S., Jestin, J., Jollivet, P. & Spalla, O. (2008). *Nat. Mater.* **7**, 978–983.
- Davidovits, J. (1991). *J. Therm. Anal.* **37**, 1633–1656.
- Desbats-Le Chequer, C. & Frizon, F. (2011). *J. Mater. Sci.* **46**, 5657–5664.
- Duxson, P., Lukey, G. C. & van Deventer, J. S. J. (2006a). *Ind. Eng. Chem. Res.* **45**, 7781–7788.
- Duxson, P., Lukey, G. C. & van Deventer, J. S. (2006b). *J. Non-Cryst. Solids*, **352**, 5541–5555.
- Duxson, P., Lukey, G. C. & van Deventer, J. S. (2007). *J. Non-Cryst. Solids*, **353**, 2186–2200.
- Duxson, P., Provis, J. L., Lukey, G. C., Mallicoat, S. W., Kriven, W. M. & van Deventer, J. S. (2005). *Colloids Surf. A Physicochem. Eng. Asp.* **269**, 47–58.
- Fernandez Jimenez, A. M., Lachowski, E. E., Palomo, A. & Macphee, D. E. (2004). *Cem. Concr. Compos.* **26**, 1001–1006.
- Fernandez-Jimenez, A., Macphee, D., Lachowski, E. & Palomo, A. (2005). *J. Nucl. Mater.* **346**, 185–193.
- Gallé, C. (2001). *Cem. Concr. Res.* **31**, 1467–1477.
- Girard, L., Arab, M. & Spalla, O. (2008). *J. Colloid Interface Sci.* **319**, 214–225.

- Ismail, I., Bernal, S. A., Provis, J. L., Hamdan, S. & Deventer, J. S. J. (2013). *J. Mater. Sci.* **48**, 3566–3577.
- Jaarsveld, J. G. S. van & van Deventer, J. S. J. (1999). *Ind. Eng. Chem. Res.* **38**, 3932–3941.
- Jämstorp, E., Forsgren, J., Bredenberg, S., Engqvist, H. & Strømme, M. (2010). *J. Controlled Release*, **146**, 370–377.
- Kuznetsova, T. F., Rat'ko, A. I. & Eremenko, S. I. (2012). *Russ. J. Appl. Chem.* **85**, 344–347.
- Kriven, W. M. & Bell, J. L. (2008). *28th International Conference on Advanced Ceramics and Composites B*, Ceramic Engineering and Science Proceedings, Vol. 25, pp. 99–104. Wiley, The American Ceramics Society.
- Kriven, W. M., Bell, J. L. & Gordon, M. (2007). *Mechanical Properties and Performance of Engineering Ceramics and Composites I*, pp. 491–503. Wiley, The American Ceramics Society.
- Lambard, J., Lesieur, P. & Zemb, T. (1992). *J. Phys. I Fr.* **2**, 1191–1213.
- Ledieu, A., Devreux, F., Barboux, P., Sicard, L. & Spalla, O. (2004). *J. Non-Cryst. Solids*, **343**, 3–12.
- Lee, W. & van Deventer, J. (2002). *Colloids Surf. A Physicochem. Eng. Asp.* **211**, 49–66.
- Leofanti, G., Padovan, M., Tozzola, G. & Venturelli, B. (1998). *Catal. Today*, **41**, 207–219.
- Lloyd, R. R., Provis, J. L. & van Deventer, J. S. (2010). *Cem. Concr. Res.* **40**, 1386–1392.
- Maitland, C. F., Buckley, C. E., O'Connor, B. H., Butler, P. D. & Hart, R. D. (2011). *J. Appl. Cryst.* **44**, 697–707.
- Mami, M., Lucas-Girot, A., Oudadesse, H., Dorbez-Sridi, R., Mezahi, F. & Dietrich, E. (2008). *Appl. Surf. Sci.* **254**, 7386–7393.
- Palomo, A. & Palacios, M. (2003). *Cem. Concr. Res.* **33**, 289–295.
- Phair, J. & van Deventer, J. (2001). *Miner. Eng.* **14**, 289–304.
- Porod, G. (1952). *Kolloid Z.* **125**, 108–122.
- Poulesquen, A., Frizon, F. & Lambertin, D. (2011). *J. Non-Cryst. Solids*, **357**, 3565–3571.
- Provis, J. L., Lukey, G. C. & van Deventer, J. S. J. (2005). *Chem. Mater.* **17**, 3075–3085.
- Prud'homme, E., Michaud, P., Joussein, E., Clacens, J., Arie-Clacens, S., Sobrados, I., Peyratout, C., Smith, A., Sanz, J. & Rossignol, S. (2011). *J. Non-Cryst. Solids*, **357**, 3637–3647.
- Radlinski, A., Mastalerz, M., Hinde, A., Hainbuchner, M., Rauch, H., Baron, M., Lin, J., Fan, L. & Thiyagarajan, P. (2004). *Int. J. Coal Geol.* **59**, 245–271.
- Ramsay, J. D. F. (1993). *Pure Appl. Chem.* **65**, 2169–2174.
- Rooses, A., Steins, P., Dannoux-Papin, A., Lambertin, D., Poulesquen, A. & Frizon, F. (2013). *Appl. Clay Sci.* **73**, 86–92.
- Rouquerol, F., Luciani, L., Llewellyn, P., Denoyel, R. & Rouquerol, J. (2003). *Techniques de l'Ingénieur Études de Structure et Caractérisation*, article P1050. Édition T.I.
- Sears, V. F. (1992). *Neutron News*, **3**(3), 26–37.
- Sharma, L., Kumar, M., Saxena, A., Chand, M. & Gupta, J. (2002). *J. Mol. Catal. A Chem.* **185**, 135–141.
- Steins, P., Poulesquen, A., Diat, O. & Frizon, F. (2012). *Langmuir*, **28**, 8502–8510.
- Steinerova, M. & Tanger, L. (2010). Nanocon 2010, 2nd International Conference, 12–14 October 2010, Olomouc, Czech Republic.
- Tsao, C., Yu, M., Chung, T., Wu, H., Wang, C., Chang, K. & Chen, H. (2007). *J. Am. Chem. Soc.* **129**, 15997–16004.
- Vance, E. R., Hadley, J. H., Hsu, F. H. & Drabarek, E. (2008). *J. Am. Ceram. Soc.* **91**, 664–666.
- Xu, J., Zhou, Y., Chang, Q. & Qu, H. (2006). *Mater. Lett.* **60**, 820–822.